Entropic interaction chromatography: Separating proteins on the basis of size using end-grafted polymer brushes

ARTICLE *in* BIOTECHNOLOGY AND BIOENGINEERING · MAY 2005

Impact Factor: 4.13 · DOI: 10.1002/bit.20430 · Source: PubMed

5 AUTHORS, INCLUDING:

Jürgen Koska
BIOVIA Dassault Systèmes
13 PUBLICATIONS **270** CITATIONS

ACCELERATED PUBLICATION

Entropic Interaction Chromatography: Separating Proteins on the Basis of Size Using End-Grafted Polymer Brushes

Peter Pang,[1,2] Jürgen Koska,[1,2] Bryan R. Coad,[3] Donald E. Brooks,[3,4] Charles A. Haynes[1]

[1]Michael Smith Laboratories, Centre for Blood Research, University of British Columbia, Vancouver, V6T 1Z3 Canada; e-mail: israels@chml.ubc.ca
[2]Department of Chemical and Biological Engineering, University of British Columbia, Vancouver, V6T 1Z3 Canada
[3]Department of Chemistry, Centre for Blood Research, University of British Columbia, Vancouver, V6T 1Z3 Canada
[4]Department of Pathology and Laboratory Medicine, University of British Columbia, Vancouver, V6T 1Z3 Canada

Received 28 September 2004; accepted 14 December 2004

Published online 10 February 2005 in Wiley InterScience (www.interscience.wiley.com). DOI: 10.1002/bit.20430

Abstract: Partitioning of a macromolecule into the interfacial volume occupied by a grafted polymer brush decreases the configurational entropy (ΔS^c_{brush}) of the terminally attached linear polymer chains due to a loss of free volume. Self-consistent field theory (SCF) calculations are used to show that ΔS^c_{brush} is a strong function of both the size (MW_p) of the partitioning macromolecule and the depth of penetration into the brush volume. We further demonstrate that the strong dependence of ΔS^c_{brush} on MW_p provides a novel and powerful platform, which we call entropic interaction chromatography (EIC), for efficiently separating mixtures of proteins on the basis of size. Two EIC columns, differing primarily in polymer grafting density, were prepared by growing a brush of poly(methoxyethyl acrylamide) chains on the surface of a wide-pore (1,000-Å pores, 64-μm diameter rigid beads) resin (Toyopearl AF-650M) bearing surface aldehyde groups. Semipreparative 0.1-L columns packed with either EIC resin provide reduced-plate heights of 2 or less for efficient separation of globular protein mixtures over at least three molecular-weight decades. Protein partitioning within these wide-pore EIC columns is shown to be effectively modeled as a thermodynamically controlled process, allowing partition coefficients (K_P) and elution chromatograms to be accurately predicted using a column model that combines SCF calculation of K_P values with an equilibrium-dispersion type model of solute transport through the column. This model is used to explore the dependence of column separation efficiency on brush properties, predicting that optimal separation of proteins over a broad MW_p range is achieved at low to moderate grafting densities and intermediate chain lengths.

Correspondence to: Dr. Charles A. Haynes
Contract grant sponsors: NSERC, Merck Biosciences Inc.; CFI grant Centre for Blood Research Chromatography (to the UBC)

Keywords: entropic interaction chromatography; size exclusion chromatography; grafted polymer brush; protein purification; equilibrium dispersion model

INTRODUCTION

Since its discovery by Porath and Flondin (1959), size exclusion chromatography (SEC), also referred to as gel permeation chromatography (GPC) in the case of lipophilic macromolecules and as gel filtration chromatography (GFC) in the case of hydrophilic macromolecules, has become a powerful method for determining molecular weight distributions and for separating mixtures on the basis of size (Yao and Lenhoff, 2004; Mathew et al., 2004; Horneman et al., 2004; Guo et al., 2003; Dubin and Principi, 1989). Due to its robustness and mild operating conditions, SEC has found broad application in the purification of biologics, including plasma proteins, monoclonal and polyclonal antibodies, nucleic acids, and a range of FDA-approved therapeutic proteins produced by recombinant DNA technology (Goetz et al., 2004; Barackman et al., 2004). In addition, SEC is commonly used for desalting and buffer exchange and as a product-polishing step for removal of impurities and undesired oligomers or aggregates (Gooding and Regnier, 1990; Barth et al., 1998). SEC was first used industrially in the desalting of dairy products (Lindquist and Williams, 1973). Since then, it has been used at preparative scales in the manufacture of insulin (Janson, 1971) and in the purification of human serum albumin (HSA) from blood plasma (Lin et al., 2000; Curling, 1980). First reported by Friedli and Kistler (1972), the removal of ethanol from HSA purified by the Cohn-Oncley cold-ethanol fractionation process remains one of

the largest and most well-documented applications of SEC (Johnston and Adcock, 2000; Bertolini et al., 2004).

Traditionally, SEC employs a porous gel or rigid porous bead as the stationary phase. Porous beads of glyceryl (diol) derivatized silica, poly(propylene oxide) or crosslinked hydroxylated polymethacrylate are widely used for biological applications (Wu, 1999). The pore size distribution within the stationary phase is well controlled during synthesis. SEC columns are therefore available packed with resin particles of either monodisperse or polydisperse pore size. The former provide high-resolution separations over a narrow range of solute size. The latter are generally of lower efficiency, but can discriminate on a log-linear basis over as much as four molecular weight decades.

Solute retention mechanisms in traditional SEC columns are usually based on hydraulic arguments, especially when describing separation of protein mixtures. In an ideal SEC column, interactions between the stationary phase and the macromolecular solutes within the pore liquid are steric in nature only, and the elution volume V_e of a solute is given by:

$$V_e = V_o + K_P V_P \tag{1}$$

where V_o is the interstitial (void) volume of the packed bed, V_p is the total volume of the pores within the stationary phase, and K_P is the solute partition coefficient, given by the ratio of a characteristic solute concentration in the pores of the stationary phase over that in the interstitial volume. K_P varies from zero for a fully excluded solute to unity for a point-like solute capable of fully and equally accessing all of the pore volume. Thus, all macromolecular solutes to be separated are expected to elute at a volume between V_o and $V_o + V_p$. Using simple geometric arguments, Ogston (1958) predicted for a monodisperse pore-size SEC resin that K_P (and therefore V_e) is a function of $\bar{r}/\bar{R}$, the ratio of the hydraulic radius of the solute to that of the stationary phase pores. This concept was later refined by Squire (1964) to include variations in solute shape and bead pore size and shape, leading to the result:

$$\frac{V_e}{V_o} = \left[1 + a\left(1 - \frac{\bar{r}}{\bar{R}}\right)\right]^3 \tag{2}$$

where a is a constant characterizing the distribution of volume within the column.

Solute retention in chromatography columns can also be described in terms of equilibrium thermodynamic arguments. Yau et al. (1979, 1989) were the first of several researchers (e.g., Dondi et al., 2002; Brooks and Müller, 1996) to show that K_P can be treated as an equilibrium constant for solute partitioning, and can therefore be related to the standard Gibbs free energy change for the partitioning process:

$$\Delta G^o = -RT \ln K_P \tag{3}$$

where:

$$\Delta G^o = \Delta H^o - T\Delta S^o \tag{4}$$

Here, ΔH° and ΔS° are the standard enthalpy and entropy changes, respectively, for transferring the solute from the interstitial phase to the pore volume of the stationary phase. In most modes of liquid chromatography (e.g., ion exchange, reversed phase, normal phase), solute partitioning is driven by strong intermolecular forces between the solute and the stationary phase. The free energy change can therefore be approximated by the enthalpy term alone. In ideal SEC, however, ΔH° is small and generally taken by definition to be zero. Thus, the distribution of a solute macromolecule between the two phases is assumed to be controlled by entropy, and:

$$K_P \equiv \exp(\Delta S^o/R) \tag{5}$$

In preparative SEC columns, the walls of the porous stationary phase matrix are usually rigid. Solute partitioning does not deform or alter the geometry of the stationary phase and ΔS° is simply the standard difference in the configurational entropy ΔS^c of the solute molecule in the stationary phase relative to that in the interstitial space, where the movement of the solute is assumed to be unconfined. The value of K_P for solute i is therefore strictly proportional to the number of unique ways solute i can occupy space within the pores of the stationary phase, since:

$$\Delta S_i^c = k \ln \frac{\Omega_i^{pore}}{\Omega_i^o} \tag{6}$$

where Ω_i^{pore} is the equally probable number of accessible configurations of solute i within the pore volume, and Ω_i^o is the analogous number for the same solute in the interstitial volume. In ideal SEC, Ω_i^{pore} is always less than Ω_i^o for any solute of size greater than the solvent, so that partitioning of a macromolecular solute i into the pores of the stationary phase always results in a decrease in ΔS_i^c. Thus, K_P is less than unity and the solute will elute before the solvent front. Equations 1, 5, and 6 predict that a small solute will be retained longer than a large solute in an SEC column because it can occupy space in the stationary phase in a larger number of configurational states. Traditional SEC therefore represents a conceptually simple but important mode of liquid chromatography where the separation is exclusively driven by relative changes in configurational entropy.

Previously, we have shown that size-based separations can also be achieved in chromatography columns packed with a stationary phase comprised of spherical *nonporous* particles bearing a grafted layer of terminally attached neutral polymer chains in a brush configuration (Brooks et al., 2000). Attachment of one end of a polymer chain to an interface leads to very distinct chain configurations and

energetics. When the end-grafted polymer is miscible in the solvent, the degree of surface coverage σ (number of grafted chains / unit area) and the degree of polymerization N_i (which in turn defines the radius of gyration R_g of the unperturbed chain i in solution) in large part determine the grafted chain conformation and properties. A crude picture of grafted chain conformation can be obtained by calculating the reduced surface coverage $\sigma^* = \pi \langle R_g^2 \rangle / \Sigma$, which gives the ratio of the cross-sectional area of the chain free in solution to the average area Σ available to chain once it is end-grafted to the surface, where $\Sigma = 1/\sigma$ and σ is the average number of chains per area. In regimes of surface coverage where $\sigma^* > 1$, grafted chain overlap occurs and the chains extend away from the surface due to steric interactions between chain segments. An end-grafted polymer layer under these conditions is termed a "brush" due to the physical picture of partially ordered, stretched linear polymers extending from a surface (Alexander, 1977; de Gennes, 1976).

As with traditional SEC, partitioning of a solute molecule into a polymer brush decreases the configurational entropy of the solute ΔS_i^c. However, as the partitioned solute occupies volume otherwise available to the end-grafted polymer, it also reduces the configurational entropy of the flexible polymer chains within the brush, so that ΔS° for the transfer of solute from the polymer-free interstitial phase to the stationary phase is now given by:

$$\Delta S^o = \Delta S_i^c + \Delta S_{brush}^c \tag{7}$$

where ΔS_{brush}^c is the change in the configurational entropy of the brush. A model of the solute–brush interaction based on self-consistent field theory (Steels et al., 2000a,b) predicts that ΔS_{brush}^c dominates ΔS° for solute partitioning into polymer brushes displayed on nonporous resin (Brooks et al., 2000) due to the very large number of configurations lost in the flexible polymer chains of the brush as volume available to the chains is decreased. The reduction in free volume scales with partitioned solute size, making ΔS_{brush}^c more negative and K_P smaller for larger solutes. The interaction of solutes with an end-grafted polymer brush phase therefore represents a new mode of liquid chromatography, which we call *entropic interaction chromatography* (EIC) to emphasize the fundamental importance of changes in configurational entropy (i.e., Eq. 7) to the separation.

Equation 7 predicts that size-based separations can be achieved in the absence of enthalpic effects through a reduction in either ΔS_i^c, ΔS_{brush}^c, or both of these quantities. Rigid-pore SEC resins, where $\Delta S_{brush}^c = 0$, and nonporous EIC resins (Brooks et al., 2000), where ΔS_i^c is small compared to ΔS_{brush}^c, therefore represent the endpoints of a spectrum of liquid chromatography modes for separating mixtures of macromolecules on the basis of size. However, resin geometries in which solute partitioning will result in the reduction of both ΔS_i^c and ΔS_{brush}^c can be envisaged. One example would be the use of porous resins bearing a brush of end-grafted neutral polymer on the pore walls. Careful control of the pore-size distribution during base resin synthesis would then allow one to specify ΔS_i^c, while tight control over the properties (grafting density, height, etc.) of the end-grafted polymer chains during brush synthesis would allow one to specify ΔS_{brush}^c. The ability to modulate the dependence of both ΔS_i^c and ΔS_{brush}^c on solute molecular weight MW_i may therefore provide the flexibility necessary to fine-tune size-based separations to meet specific needs. Porous EIC resins should have a number of additional advantages over the nonporous version of EIC we previously described and characterized (Brooks et al., 2000). In particular, porous resin geometries will greatly improve stationary-phase capacity, permitting the use of larger diameter resin particles to reduce column pressure drop and increase throughput.

In this article we describe the performance of two entropic interaction chromatography columns incorporating a porous stationary phase with the intent of extending our previously validated EIC technology to preparative-scale separations. Both columns display a poly(methoxyethyl acrylamide) (PMEA) brush on the walls of the 1,000-Å pores of a rigid particulate resin. With chemistry and properties similar to a commercial form of EIC (the Fractogel BioSEC column of E. Merck KGaA), the two columns differ primarily in the grafting density of the PMEA brush. A model for predicting elution chromatograms and selectivity curves from these and related porous EIC columns is developed by introducing the total configurational entropy change ΔS° into an equilibrium-dispersion type chromatography model. Values of ΔS° are calculated as a function of solute and brush geometry using the numerical self-consistent-field (SCF) model of Steels et al. (2000a). Changes in the configurational entropy of the partitioned solutes are not considered in the model since the 1,000-Å pores of the base resin used in the two EIC columns characterized in this study are significantly larger than the hydraulic radii of the proteins to be separated. Thus, $\Delta S_i^c \approx 0$ and no separation is predicted by a classic SEC model (Eq. 2) or *experimentally observed* in the absence of the end-grafted polymer brush. This simplified model is first validated through comparison with elution and selectivity data from the two EIC columns and then used to predict how the separation efficiency of porous EIC is affected by changes to the properties of the end-grafted brush.

MODELING OF LARGE-PORE ENTROPIC INTERACTION CHROMATOGRAPHY

Solute Transport Equations

Our model for solute transport through large-pore (and also nonporous) EIC columns is based on a configurational entropy controlled size-exclusion mechanism. The EIC column of length L and diameter d_c is assumed to be

uniformly packed, so that solute concentrations and solvent and solute transport vary only in the z direction, which defines the central axis of the cylindrical column. The flux of a given solute through the column can then be expressed by a generalized continuity equation that includes contributions from convection, solute partitioning into the stationary phase, and solute dispersion in the axial direction due to transport nonidealities:

$$\left(1+\frac{(1-\varepsilon)}{\varepsilon}\frac{\partial q}{\partial c}\right)J = \left(1+\frac{(1-\varepsilon)}{\varepsilon}K_P\right)J = -D\frac{\partial c}{\partial z}+u_o c \qquad (8)$$

where J is the solute flux (mol m^{-2} s^{-1}), D is the effective axial dispersion coefficient (m^2 s^{-1}), c is the solute concentration (mol m^{-3}) in the mobile phase, q is the corresponding equilibrium concentration of solute in the stationary phase, and u_o is the solvent velocity (m s^{-1}). For creeping flow within a uniformly packed column of equal-sized spherical resin particles, axial solute dispersion can be related to the molecular diffusivity D_m of the solute in an unconfined solution by:

$$D = a\frac{D_m}{\tau} \qquad (9)$$

where τ, the tortuosity factor, is 1.4 for the interstitial spaces between hexagonally packed spherical particles, and a is a proportionality constant equal to unity (Athalye et al., 1992). At higher flows where the Peclet number Pe (also known as the reduced velocity) is greater than 1, the proportionality constant a takes on values greater than unity, and the value of D then empirically accounts for peak spreading due to all forms of nonideal solute transport in the column. Molecular diffusivities were estimated using the correlation of Tyn and Gusek (1990), who found that D_m values for globular proteins are directly proportional to temperature and inversely proportional to solvent viscosity and hydraulic radius.

Equation 8 assumes separation within the column is thermodynamically controlled according to the linear isotherm. Discrimination of dissimilar macromolecular solutes by the matrix is controlled by differences in the value of K_P for each species. Kinetic models of chromatography that more explicitly account for the impact of the stationary phase on solute transport could, of course, be used. These more mathematically intensive models may in fact be necessary to model EIC resins containing a highly constraining pore structure that results in intraparticle diffusivities being appreciably smaller than D_m. However, for the large-pore columns described in this work solute partitioning is dominated by equilibrium solute exchange between the mobile and stationary phases. Here it is important to note that a solute macromolecule, or even a pulse of these molecules, migrating through the chromatography column need not achieve the condition of equilibrium exchange at the length scale of a single resin particle for Eq. 8 to apply. Instead, equilibrium exchange must be established only prior to elution of the solute from the column. The column length required for equilibrium solute exchange defines the height equivalent to one theoretical plate (*HETP*), and we will show that the *HETP* in our wide-pore EIC columns is orders of magnitude less than the column length. For the equilibrium-dispersion model defined by Eq. 8, the *HETP* is given by:

$$HETP = \frac{2d_p}{Pe} = \frac{2d_p}{\left(d_p u_o/D\right)} \qquad (10)$$

where Pe is the particle-level Peclet number and d_p is the resin particle diameter (m).

Assuming enthalpic interactions between the solute and the chromatographic matrix are negligible, the solute equilibrium constant K_P given by Eq. 5 can be simplified to:

$$K_P = \exp\left(\frac{\Delta S^c_{brush}}{R}\right) \qquad (11)$$

since $\Delta S^c_{brush} \gg \Delta S^c_i$ due to the large pores of the base matrix. A method for accurately estimating ΔS^c_{brush} (or equivalently K_P) would therefore allow solution of Eq. 8 for J and c. In this work, Eq. 8 is solved numerically using a standard forward-backward finite difference scheme setting the number of volume elements equal to the number of theoretical plates within the column (Guiochon et al., 1994). The mean solute velocity u through the column is then determined as:

$$u = \frac{\int J(z)dz}{\int c(z)dz} \qquad (12)$$

along with the profile of the solute elution peak. All model calculations are based on a pulse feed specified by the initial condition:

$$c(t=0,z) = \frac{m}{A\varepsilon}\delta(z) \qquad (13)$$

and standard column chromatography boundary conditions (Danckwerts, 1953). In Eq. 1), m (kg) is the mass of solute injected as a pulse into the column at position $z = 0$, A (m^2) is the cross-sectional area of the column, ε is the interstitial void fraction, and $\Delta(z)$ is the Dirac delta function.

Estimation of ΔS^c_{brush} Using SCF Theory

Steels et al. (2000a) developed a numerical self-consistent field (SCF) theory to calculate the segment-density distribution of end-grafted polymer brushes around a macromolecular particle positioned at various distances from the grafting surface. Their model is based on the original SCF model for polymer adsorption developed by Scheutjens and Fleer (1979, 1980), and places a brush of end-grafted chains in a cylindrical lattice geometry where the impenetrable grafting surface is positioned at layer $x = 1$. This

lattice geometry therefore provides a grafting surface at one end of a cylinder from which polymer chains extend into the solution in the x direction. The undisturbed brush is completely uniform in the radial r direction and displays a nonuniform segment density in the x direction. An impenetrable solute particle may then be centered on the lattice axis at some distance x_p from the grafting surface and moved toward that surface to compute the energetics of solute partitioning. For convenience, a cylinder of radius r_p and length l_p is used for the particle in all simulations reported here.

The numerical SCF model considers the partitioning of an individual particle and is therefore strictly valid only at dilute solute conditions. However, by definition K_P is constant over a broad range of solute concentrations, making model estimates valid at normal column operating conditions. Our objective therefore is to adapt the model of Steels et al. (2000a) to estimate ΔS^c_{brush} (or K_P) for the partitioning of an impenetrable macromolecular solute into the PMEA brush volume of an EIC column as a function of brush properties, solvent quality, and solute particle size. All details concerning the basic derivation and numerical solution of the model are provided in Steels et al. (2000a). We therefore restrict our attention to an explanation of how the model may be used to estimate ΔS^c_{brush} and K_P.

The independent variables in the SCF model are the system composition, volume, and temperature. Thermodynamic equilibrium is therefore achieved in the simulation by minimizing the Helmholtz energy A, which is determined through calculation of the canonical partition function Q:

$$\frac{A - A^*}{kT} = -\ln\left(\frac{Q}{Q^*}\right) = \left(\frac{U - U^*}{kT}\right) - \ln\left(\frac{\Omega}{\Omega^*}\right) \qquad (14)$$

where superscript * represents the reference state, taken here as the pure components at system temperature. The two terms on the right side of the last equality specify the energetic U and entropic contributions to Q. To evaluate Q, both contributions are expressed in terms of parameters available from the self-consistent lattice model:

$$-\ln\left(\frac{Q}{Q^*}\right) = \sum_x \sum_r \sum_i L(r) \times \left(\sum_{j=i+1}^{m} \Phi_i(x,r)\chi_{ij} \left\langle \Phi_j(x,r) \right\rangle - \Phi_i(x,r) \times \left\{ \frac{\ln \Phi_i^{\infty}}{N_i} + \ln G_i(x,r) \right\} \right) \qquad (15)$$

where $L(r)$ is the area in lattice units of radial r, $\Phi_i(x,r)$ is the volume fraction of component i in radial (x,r) (the volume fraction in the mobile phase is denoted by the superscript ∞), χ_{ij} is the Flory interaction parameter for components i and j, N_i is the degree of polymerization of component i, and $G_i(x,r)$ is the Boltzmann-type weighting factor for moving component or chain segment i to position (x,r) in the lattice.

In our SCF simulations, the particle p is initially positioned in the lattice outside the brush volume ($x_p = \infty$, where x_p is the position of the lower edge of the cylindrical particle) and moved stepwise toward the grafting surface. A self-consistent solution to Eq. 1) is obtained at each particle position. At all x_p values greater than the unperturbed brush height (h), solution of Eq. 15 yields a constant value of $(A - A^*)/kT$, where $A = A^{\infty}$ and represents the Helmholtz energy of the system when the particle is unconfined (i.e., when the particle is partitioned into the mobile phase). For all $x_p \leq h$, the Helmholtz energy of the system depends on x_p due to the change in grafted-polymer segment density with distance from the grafting surface. Solving Eq. 15 therefore allows calculation of the Helmholtz energy change $\Delta A(x_p)$ associated with partitioning of the particle to position x_p:

$$\Delta A(x_p) = (A(x_p) - A^*) - (A^{\infty} - A^*) \qquad (16)$$

The SCF model does not account for changes in the configurational entropy of the particle (ΔS^c_i) due to partitioning, since the particle position is fixed in these calculations. Instead, it calculates the equilibrium response of the brush to the introduction of the particle into the brush volume. In all calculations reported here, the brush (b) – particle (p) interaction is assumed athermal and χ_{bp} is set equal to zero. Provided the brush solvent interaction is relatively weak, we then find that $\Delta A(x_p) \approx -T\Delta S^c_{brush}(x_p)$. The average solute partition coefficient can therefore be determined by solving Eq. 11 for each particle position and integrating over the entire height of the brush (h is specified in this work as the x value where the polymer-segment volume fraction in the undisturbed brush falls below 0.1%):

$$K_P = \frac{\int_{x=1}^{h} K_P(x_p)dx}{\int_{x=1}^{h} dx} = \frac{\int_{x=1}^{h} \exp\left(\Delta S^c_{brush}(x_p)/_R\right)dx}{\int_{x=1}^{h} dx} \qquad (17)$$

MATERIALS AND METHODS

EIC Columns

Wide-pore EIC columns were prepared using Toyopearl AF Formyl-650M as the base matrix. Toyopearl AF Formyl-650M is a hydrophilic, dimensionally stable matrix with uniform 1,000-Å pores that have a globular-protein exclusion limit of 5,000,000 Da. The base matrix provides no size-based separation of proteins or other macromolecules less than 1,000,000 Da (data not shown). The aldehyde functional group density within the matrix was specified by the manufacturer to be 60 μmol mL^{-1}. Resins of lower aldehyde density appropriate for EIC

grafted-brush synthesis were prepared by adding appropriate amounts of $NaCNBH_3$ to the resin suspension and gently agitating for 14 h at 4°C. The resulting aldehyde density was determined by mass balance after washing the resin with 1 M NaCl, decomposing the cyanic content of the solution with sodium hypochlorite, and analyzing by gas chromatography.

The Toyopearl resin slurry was washed with 20 volumes of water to remove the 0.02% sodium azide used as a preservative during storage. A grafted brush of poly(methoxyethyl acrylamide) (PMEA) was then introduced onto the walls of the base resin using a cerium (IV) catalyzed polymerization reaction at conditions similar to those described in our previous work (Brooks et al., 2000). Total MEA content was determined from the uptake of monomer as assessed by reversed-phase HPLC of the supernatants. The final unreacted aldehyde content of the resin was determined (and blocked) by titration with either $NaCNBH_3$ or hydroxylamine hydrochloride as described above or in Brooks et al. (2000), respectively. Homogeneous distribution of monomer between all reacted aldehyde groups on the base matrix was then assumed to compute the average degree of polymerization of the brush.

Table I lists measured properties of the two columns (AF650M-PMEA5 and AF650M-PMEA12) prepared for this study. In each case, the synthesized resin was loaded at room temperature into a 60 cm (length) by 1.5 cm (diameter) jacketed column as a 10% slurry in 1 M NaCl at a packing velocity of 0.2 cm s^{-1}. The range of particle diameters and the average d_p of the EIC resin was determined by imaging more than 100 EIC particles using an inverted microscope (Axiovert 100, Carl Zeiss, Oberkochen, Germany) equipped with a monochrome solid-state camera (COHU, San Diego, CA) connected to a real-time frame-grabber (Visionplus-AT, Imaging Technology, Woburn, MA). The column diameter to particle diameter ratio of 250 is well above the minimum value required to safely ignore additional dispersion effects that may occur at the column wall (Knox et al., 1976). Evidence that each wide-pore EIC resin is packed uniformly within the column is provided by two experimental measures of column packing efficiency, the reduced plate height h and the peak asymmetry factor A_s. For an efficiently packed column, the reduced plate height should be close to 2 and the asymmetry factor should be close to unity (Bristow and Knox, 1977).

Pressure drop across the column was monitored as a function of u_o to estimate the interstitial void fraction of the column. Application of the Blake, Kozeny, and Carmen equation (Allen, 1981):

$$\Delta P = 36k \frac{u_o}{\varepsilon} \frac{L\eta}{d_p^2} \frac{(1-\varepsilon)^2}{\varepsilon^3} \tag{18}$$

to column pressure drop (ΔP, Pa) data yields a column resistance factor, defined as $36k(1–\varepsilon)^2/\varepsilon^3$, of 1,100 ± 40. For spherical packing, the aspect factor k is assumed equal to 5 (Janson and Jonsson, 1998). The porosity β of the stationary phase was then determined by potassium nitrate (KNO_3) elution behavior as described by Hagel (1989).

Table I. Measured parameters and properties for the two entropic interaction chromatography columns prepared and used in this work.

Column property	Column		Units
	AF650M-PMEA5	AF650M-PMEA12	
Temperature	20	20	°C
L	60	60	cm
d_c	1.5	1.5	cm
d_p	64 ± 13	64 ± 13	μm
ε	0.29 ± 0.03	0.30 ± 0.02	
β	0.70 ± 0.02	0.63 ± 0.03	
σ[a]	5.2	11.7	
$<N_{brush}>$[b]	240	217	
Pe	25 to 300	25 to 300	
N[c]	1550 ± 35	1200 ± 40	
h (reduced plate height)[d]	1.7 ± 0.2	2.1 ± 0.1	
A_s (peak asymmetry factor)[e]	1.04 ± 0.02	1.06 ± 0.03	

[a]Calculated based on $NaCNBH_3$ titration data as described in the text.

[b]Calculated based on mass balance assuming all MEA reacted was distributed on the beads and assuming that all grafted chains in the brush are the same length and all available grafting sites bear a chain of that length.

[c]Based on peak width w at baseline data for KNO_3 elution.

[d]The reduced plate height h, defined as $HETP/d_p$, was calculated from elution data for sodium nitrate (u_o = 0.0254 cm s^{-1}) using the relation $h = L/[5.54(V_e/w)^2 d_p]$ originally proposed by Van Deemter et al. (1956).

[e]Calculated from the elution peak for sodium nitrate (u_o = 0.0254 cm s^{-1}) at 10% peak height according to the method of Hagel (1989).

Measurement of Chromatograms and Selectivity Curves for Globular Proteins

Macromolecules used in this study were purchased from Aldrich Canada and include insulin (5.8 kDa, 12.4 Å, 5.3), α-lactalbumin (14.4, 17.3, 4.8), myoglobulin (17.6, 17.2, 7.0), trypsin inhibitor (20.1, 18.5, 4.5), carbonic anhydrase (29, 20.7, 7.0), β-lactoglobulin A (36.6, 21.6, 5.1), ovalbumin (43, 23.4, 4.6), BSA (67, 27.2, 4.9), conalbumin (77, 29.1, 6.6), alcohol dehydrogenase (150, 35, 5.4), aldolase (158, 35.1, 7.8), β-amylase (200, 37.6, 4.2), catalase (232, 39.8, 5.7), ferritin (440, 63, 6.6), apoferritin (443, 68), thyroglobulin (669, 85, 4.6), and blue dextran (2,000). When applicable and available, the molecular weight (kDa), radius of gyration (Å) and isoelectric point of each analyte are provided in that order in the bracket following the analyte name. Chromatograms were measured at room temperature using an AKTA Explorer 100 (Amersham Biosciences, Arlington Heights, IL) equipped with one of the EIC columns preequilibrated with elution buffer (20 mM Tris-HCl + 100 mM NaCl, pH 8). The 500 μL of sample containing 1–5 mg mL^{-1} of total protein in elution buffer was pulse injected onto the column and eluted isocratically with 20 mM Tris-HCl + 100 mM NaCl, pH 8, at a flowrate of 0.5 mL min^{-1} to 3 mL min^{-1} while monitoring at 280 nm. The partition coefficient of each analyte was calculated as $K_P = (V_e - V_o)/(V_p)$ where V_p, the pore volume of the stationary phase, was estimated as the difference in the elution volumes of KNO_3 and blue dextran.

RESULTS AND DISCUSSION

Performance of Wide-Pore EIC

At all eluent flowrates, measured chromatographic peaks for KNO_3 and for each protein studied are Gaussian or nearly Gaussian in shape with a peak aspect ratio near unity (e.g., Fig. 1). V_e and peak width w at baseline data for KNO_3 elution show that EIC columns AF650M-PMEA5 and AF650M-PMEA12 offer theoretical plate counts (N, i.e., number of theoretical plates) of ~1,550 and 1,200, respectively, where $N = 16(V_e/w)^2$. While plate counts in excess of 10,000 can be achieved in long analytical SEC columns packed with resin particles of $d_p < 5$ μm, N is predicted to drop with resin particle size. When solute diffusion limits column efficiency, for example, Ladisch (2001) has shown that N is proportional to $L/(u_o d_p^{1.5})$, where L is column length. For preparative-scale columns packed with 50–80 μm d_p particles, such as the ones described here, an N in excess of 1,000 for a 60-cm column is therefore indicative of a highly efficient separation mode. This is demonstrated by the chromatogram shown in Figure 1, where a mixture of thyroglobulin, ovalbumin, and α-lactalbumin is baseline separated on EIC column AF650M-PMEA5.

For each EIC column, Figure 2 shows the selectivity curve constructed from elution data measured at a mobile-phase flow rate of 1 mL min^{-1}. Both selectivity curves are linear over at least three orders of magnitude of solute molecular weight. As expected, the higher brush density AF650M-PMEA12 resin excludes proteins more strongly, resulting in lower partition coefficients and faster elution times. The superior throughput of this higher density resin is balanced by its lower resolving power for analytes of MW greater than 10 kDa, as indicated by the less steep linear portion of the selectivity curve relative to that for column AF650M-PMEA5. However, solute partitioning in the high-density resin shows a strong dependence on molecular weight for solutes less than 10 kDa, indicating that AF650M-PMEA12 is the more efficient column in this molecular-weight region.

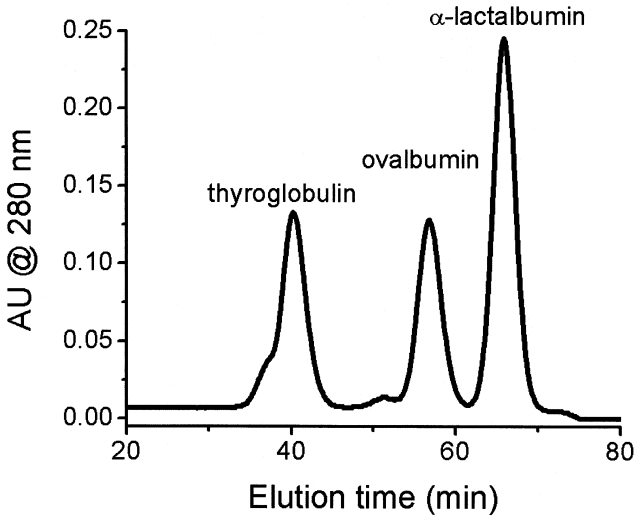

Figure 1. Elution chromatogram for a mixture of thyroglobulin, ovalbumin, and α-lactalbumin injected as a 500 μL pulse onto EIC column AF650M-PMEA5 operated at 20°C and a mobile phase (20 mM Tris-HCl buffer + 100 mM NaCl, pH 8) flow rate of 1 mL min^{-1}.

Validation of EIC Column Model and Thermodynamically Controlled Retention Mechanism

As first specified by Yau et al. (1979), a large N is one of two performance criteria that must be satisfied to model solute retention in an SEC (or an EIC) column using a simple equilibrium-dispersion model that does not explicitly account for intraparticle resistances to solute transport. The second is that both V_e and elution peak shape are independent of flow rate, making D concentration independent. Normalized elution peaks for α-lactalbumin from EIC column AF650M-PMEA5 were found to be independent of u_o over a 4-fold increase in solvent velocity (Fig. 3). Similar results were obtained with EIC column AF650M-PMEA12, indicating that solute partitioning and retention in either column can be modeled as a thermodynamically controlled process where the equilibrium plate height is determined by a combination of mass-transfer resistances embodied in D, the lumped solute dispersion coefficient.

Figure 4 compares α-lactalbumin and trypsin inhibitor elution peaks from the AF650M-PMEA5 column with

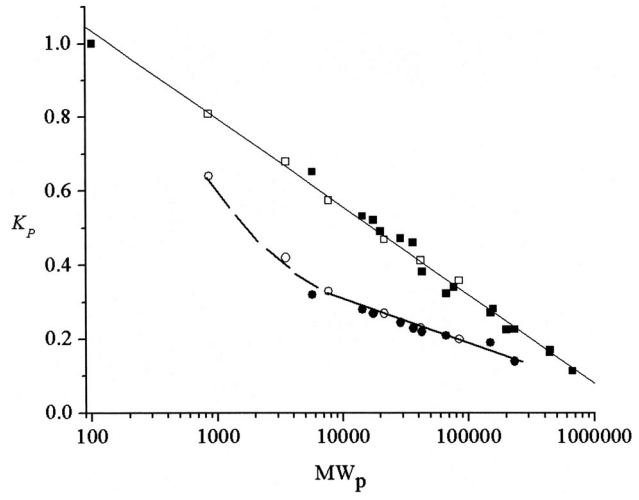

Figure 2. Measured selectivity curves for EIC columns AF650M-PMEA5 (filled squares) and AF650M-PMEA12 (filled circles) constructed from globular protein elution data at a mobile-phase flow rate of 1 mL min^{-1} and an operating temperature of 20°C. Proteins eluted from each column include insulin (MW = 5.8 kDa, R_G = 12.4 Å), α-lactalbumin (14.4, 17.3), myoglobulin (17.6, 17.2), trypsin inhibitor (20.1, 18.5), carbonic anhydrase (29, 20.7), β-lactoglobulin A (36.6, 21.6), ovalbumin (43, 23.4), BSA (67, 27.2), conalbumin (77, 29.1), alcohol dehydrogenase (150, 35), aldolase (158, 35.1), β-amylase (200, 37.6), catalase (232, 39.8), ferritin (440, 63), apoferritin (443, 68), and thyroglobulin (669, 85). EIC-SCF model predictions of selectivity curves for EIC columns AF650M-PMEA5 (open squares and line) and AF650M-PMEA12 (open circles and curved line) are also shown.

those estimated from solution of Eq. 8, hereafter referred to as the EIC-SCF model. Good agreement is observed, both in terms of elution volumes and overall peak shapes, when N_{brush} is set equal to 50. K_P values used in the model were based on solution of Eqs. 14–17. Convergence of calculated K_P values with experiment was observed by

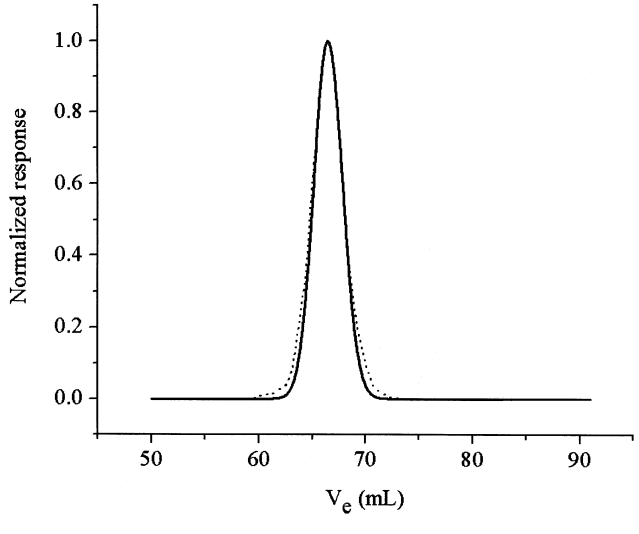

Figure 3. Normalized elution peaks from EIC column AF650M-PMEA5 for a 500-μL pulse of α-lactalbumin injected at different solvent velocities u_o: 1.57×10^{-4} m s^{-1} (solid line), 6.2×10^{-4} m s^{-1} (dashed line).

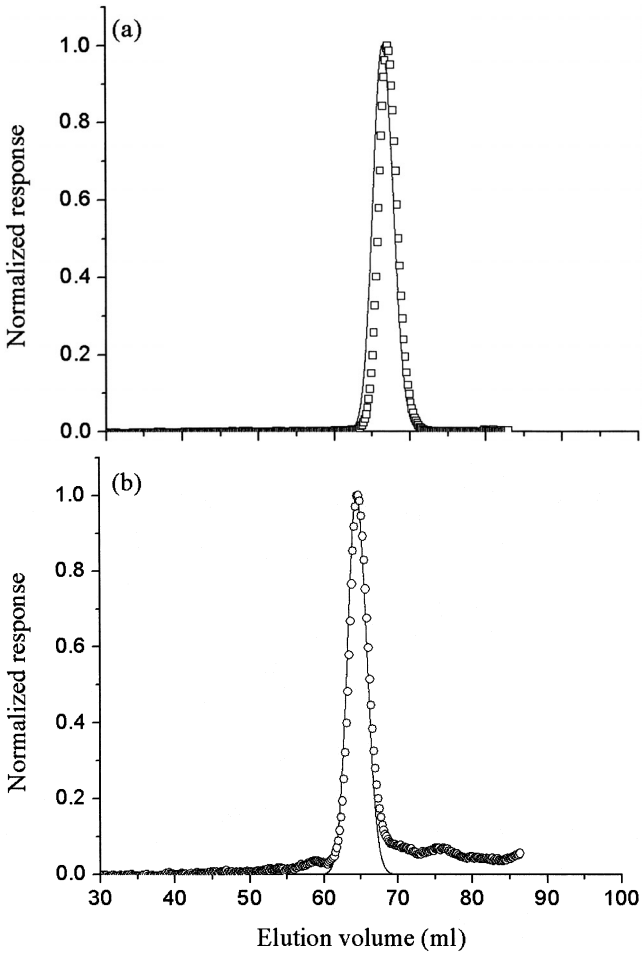

Figure 4. Comparison of protein elution peaks from the AF650M-PMEA5 column with those predicted by our EIC-SCF model (solid curves). **a:** α-Lactalbumin (open squares). **b:** Trypsin inhibitor (open circles). Model calculations based on protein molecular diffusivities estimated from the correlation of Tyn and Gusek (1990), a = 1.3, and N_{brush} = 50.

allowing each lattice site to be occupied by four amino acids. The radius r_p (lattice units) of the model cylindrical solute particle then scales with protein molecular weight according to:

$$MW = 400(\pi r_p^3)^{\frac{2}{3}} \tag{19}$$

where 400 is a constant representing the average molecular weight of the tetrapeptide within each protein-occupying lattice site. These scalings of protein and brush sizes were then fixed and used to predict selectivity curves for both the AF650M-PMEA5 column, data from which was used to define both N_{brush} and Eq. 19, and the AF650M-PMEA12 column, from which no data was used to scale brush and particle sizes within the model (Fig. 2). Thus, while the good agreement of the model with the experimental selectivity curve for the AF650M-PMEA5 column is correlative in nature, that with the selectivity curve for the AF650M-PMEA12 column demonstrates the model's predictive capabilities.

The predictive power of our proposed EIC model suggests that it can be useful in describing the nature of the protein–brush interaction and the dependence of column performance on brush and solvent properties. For example, Figure 5a reports calculated values of $\Delta S^c_{brush}(x)$ for different sized solutes penetrating into a 5% grafting density brush such as that displayed in EIC column AF650M-PMEA5. This result, which defines the molecular and entropic basis for entropic interaction chromatography, indicates that $\Delta S^c_{brush}(x)$ is a strong function of both particle size and particle position within the grafted polymer brush. Brush configurational entropy is lost as an impenetrable solute particle partitions further into the brush volume. This effect scales strongly with particle size such that for a particle positioned at $x_p = 12$, $-\Delta S^c_{brush} x_p$ is ~ 30 times larger when $r_p = 10$ than when $r_p = 2$.

The remainder of this work explores the dependence of EIC separation efficiency, defined in terms of the predicted selectivity curve, on those variables that can be controlled during resin synthesis or column operation: namely, grafting density σ, N_{brush}, and solvent quality, which enters the model through the values of χ_{bo} and χ_{po}.

Effect of Polymer Grafting Density

The selectivity curves shown in Figure 2 indicate that solute partitioning in wide-pore EIC columns is a strong function of σ, as might be expected by the known dependence of brush configurations and energetics on grafting density. Figure 2 also shows that the dependence of solute partitioning on σ is captured by our EIC-SCF model. Segment density profiles for terminally attached polymer brushes of grafting density less than 8% have been measured by small-angle neutron scattering (Cosgrove et al., 1987) and by neutron reflectivity (Field et al., 1992; Cosgrove et al., 1991). For end-grafted brushes of nonadsorbing linear homopolymer, Φ_{brush} exhibits a maximum several nanometers from the grafting surface and then decreases slowly and parabolically away from the surface. At low grafting densities ($\sigma < 6\%$), the parabolic nature of the decrease in $\Phi_{brush}(x)$ is lost near the outer edge of the brush, where Φ_{brush} decreases very slowly, giving rise to an extended tail region. As shown in Figure 5b, the SCF model of Steels et al. (2000a) captures this known dependence of Φ_{brush} on x, predicting for a 5% grafting-density brush a depletion layer next to the grafting surface, leading to a parabolic maximum in the segment density that terminates in an extended tail region. Similar results are obtained from both Monte Carlo (Chakrabarti and Toral, 1990; Lai and Binder, 1992) and molecular dynamics (Murat and Grest, 1996) simulations.

Comparison of Figure 5a,b reveals that $-\Delta S^c_{brush}(x)$ scales with $\Phi_{brush}(x)$ for partitioning of a solute particle into lattice layers near the surface of the unperturbed brush. Changes in brush configurational entropy are therefore relatively small for solute partitioning to positions near the surface region of the brush where $\Phi_{brush}(x)$ is low. Larger values of $-\Delta S^c_{brush}(x)$ are predicted for solute partitioning to positions closer to the grafting surface where the brush is considerably denser. $K_P(x)$ is therefore largest (i.e., closest to unity) in those brush layers in which $\Phi_{brush}(x)$ is small and tends toward zero with increasing particle penetration. The dashed line in Figure 5a identifies the minimum value of $-\Delta S^c_{brush}(x_p)/k$ (~ 9) for which $K_P(x) < 0.0001$. Solute

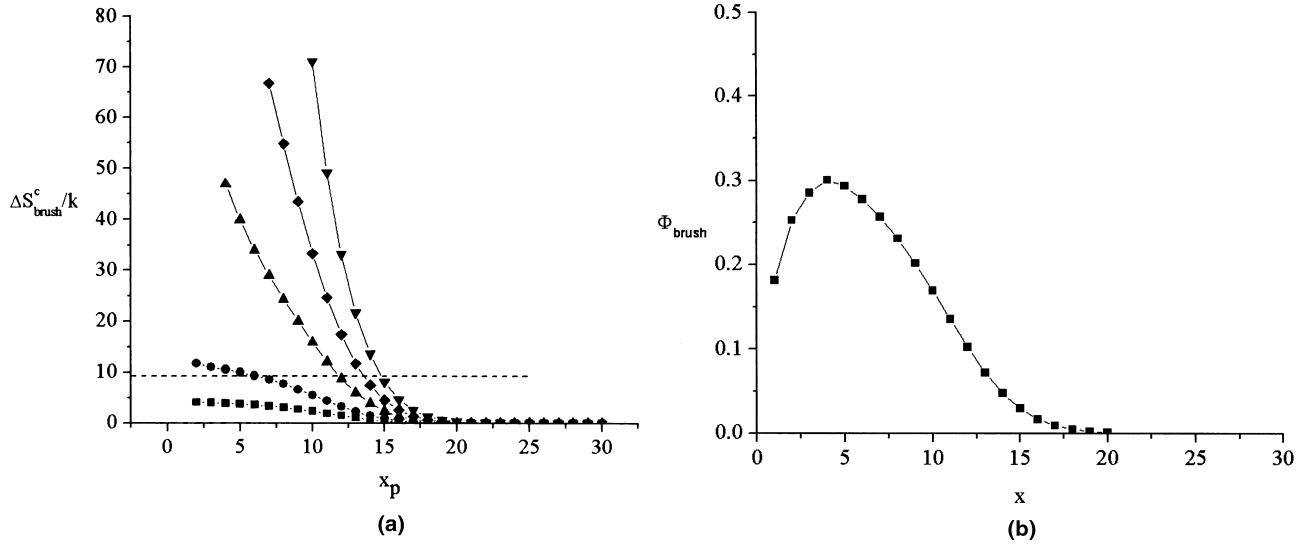

Figure 5. Predicted properties of a 5% grafting density brush. **a:** The dependence of ΔS^c_{brush} on particle penetration, where x_p represents the position of the leading face of the cylindrical particle, for different sized solutes penetrating into a 5% grafting density brush where $N_{brush} = 50$, $\kappa_{bp} = 0$, and $\kappa_{bo} = \kappa_{po} = 0.4$. Particle radii are 2 (filled squares), 3 (filled circles), 5 (filled triangles), 7 (filled diamonds), and 10 (filled inverted triangles). All solutes are symmetric in shape with $r_p = L_p$. The dashed horizontal line identifies the minimum value of $-\Delta S^c_{brush}(x_p)/k$ for which $K_P(x) < 0.0001$. **b:** Polymer segment density $\Phi_{brush}(x)$ profiles within the undisturbed 5% grafting density polymer brush ($N_{brush} = 50$, $\kappa_{bo} = 0.4$).

partitioning to this layer x or positions closer to the grafting surface is therefore negligible compared to the average value of K_P for positions between layer x and the free surface of the brush. Small solutes ($r_p \leq 2$) access essentially the entire volume of the 5% brush. Moreover, the depth of the brush into which appreciable solute partitioning occurs is predicted to diminish relatively slowly with increasing solute size, giving rise to an efficient column characterized by a relatively steep selectivity curve.

Solute partitioning (Fig. 6a) and segment density profiles (Fig. 6b) are appreciably different for a brush of grafting density $\sigma = 12\%$. As σ increases, the brush is predicted to stretch away from the grafting surface. The degree of chain stretching is determined by a balance between the loss in chain entropy as it extends into a linear configuration, and the gain in polymer-segment stepping paths when adjacent lattice sites become occupied by solvent. When $\sigma = 12\%$, the brush segment density is predicted to become more parabolic in shape, so that $\Phi_{brush}(x)$ increases rapidly at depths just beneath the free surface of the brush. As a result, partitioning of all but the smallest solutes is effectively restricted to regions near the surface of the brush. Less of the brush volume is then active in the separation process (except with respect to very small analytes), and both K_P values and the selectivity of the column are reduced.

This is not to say that high-density wide-pore EIC resins have no value. The strong dependence of K_P on molecular weight in the low molecular-weight solute regime, combined with the near exclusion of moderate to high molecular weight solutes from the brush volume, suggests that AF650M-PMEA12 and higher density resins may be useful for rapid and efficient desalting of macromolecular products such as proteins or oligonucleotides. Shorter elution times, decreased sample dilution, and a reduction of sample loss due to nonspecific interactions with the stationary matrix should be realized.

Effect of Polymer Chain Length

Figure 7a shows the EIC-SCF model results for the dependence of column selectivity on polymer chain length when $\sigma = 5\%$. Increasing chain length is predicted to decrease partitioning of solutes into the brush due to the increased entropic repulsion arising from the larger number of chain segments. Linear selectivity curves are predicted for short ($N_{brush} = 25$) to medium ($N_{brush} = 50$) length brushes, with the steepness of the slope increasing with increasing N_{brush}. The column separation efficiency is improved because the decrease in K_P with increasing N_{brush} intensifies with increasing solute molecular weight. An appreciation of why this occurs can be gained from the segment density profiles for the undisturbed brushes (Fig. 7b). Brush height increases approximately linearly with N_{brush}, expanding the brush volume without increasing significantly the maximum segment density within the brush. As previously noted, partitioning occurs to brush lattice layers where $-\Delta S^c_{brush}(x_p)/k < \sim 9$. Very small solutes can therefore partition to most layers of the brush volume, irrespective of N_{brush} and the resulting brush height. In contrast, the fraction of the total brush volume to which a large solute can partition decreases with increasing N_{brush}, due primarily to the relatively rapid increase in $\Phi_{brush}(x)$ with decreasing x away from the brush surface.

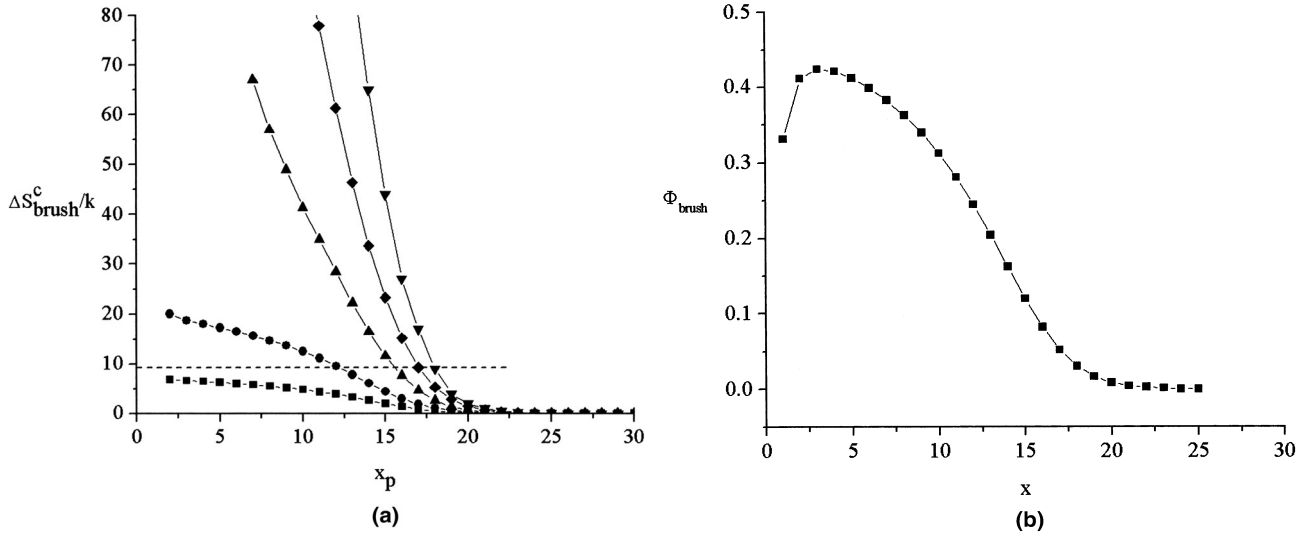

Figure 6. Predicted properties of a 12% grafting density brush. **a:** The dependence of ΔS^c_{brush} on particle penetration, where x_p represents the position of the leading face of the cylindrical particle, for different sized solutes penetrating into a 12% grafting density brush where $N_{brush} = 50$, $\kappa_{bp} = 0$, and $\kappa_{bo} = \kappa_{po} = 0.4$ Particle radii are 2 (filled squares), 3 (filled circles), 5 (filled triangles), 7 (filled diamonds), and 10 (filled inverted triangles). All solutes are symmetric in shape with $r_p = L_p$. The dashed horizontal line identifies the minimum value of $-\Delta S^c_{brush}(x_p)/k$ for which $K_P(x) < 0.0001$. **b:** Polymer segment density $\Phi_{brush}(x)$ profiles within the undisturbed 5% grafting density polymer brush ($N_{brush} = 50$, $\kappa_{bo} = 0.4$).

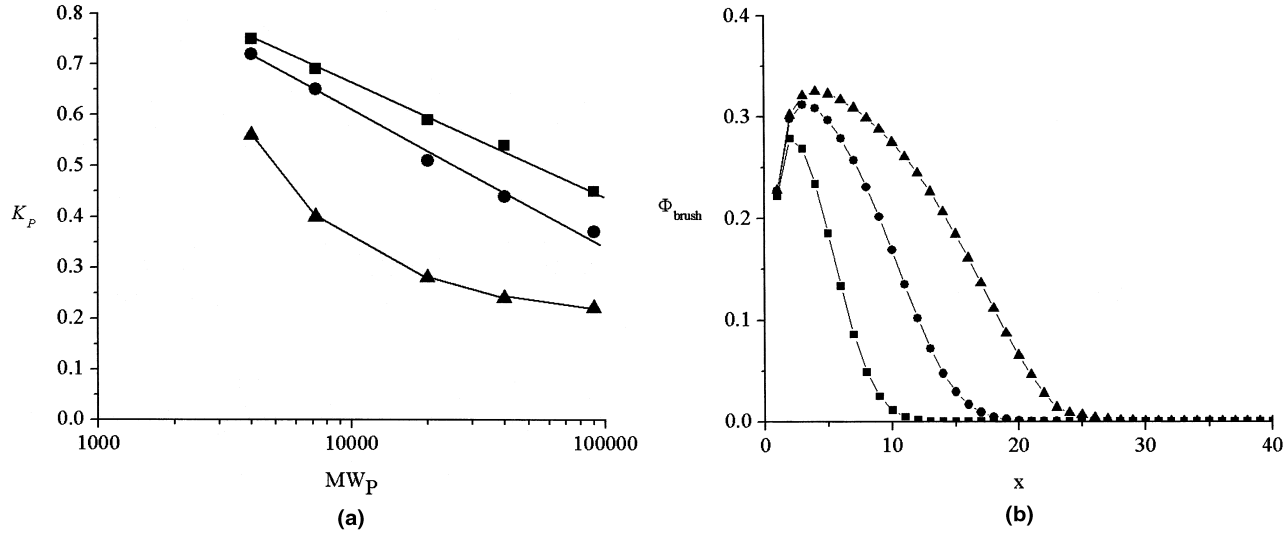

Figure 7. EIC column performance as a function of polymer brush chain length. **a:** SCF-EIC model predictions of the dependence of column selectivity on polymer chain length (σ = 5%, κ_{bo} = κ_{po} = 0.4, κ_{bp} = 0): N_{brush} = 25 (filled squares), 50 (filled circles), 100 (filled triangles). **b:** Influence of brush chain length N_{brush} on predicted segment density profiles for an undisturbed grafted-polymer brush (σ = 5%, κ_{bo} = 0.4): N_{brush} = 25 (filled squares), 50 (filled circles), 80 (filled triangles).

For an end-grafted brush of monodisperse polymer, maximum separation efficiency is predicted at an intermediate chain length. As shown in Figure 7a, the selectivity curve for N_{brush} = 100 shows significant curvature, predicting poor resolution of high molecular weight protein mixtures due to the vanishingly small percentage of the total brush volume into which they partition. One could argue that EIC columns displaying long polymer brushes could be useful for removing low molecular solutes from a complex mixture. Our results suggest, however, that EIC removal of low MW analytes can be achieved more efficiently by decreasing N_{brush} while increasing σ, which allows retention of low MW species while minimizing elution volumes and peak spreading for rejected high MW species.

Effect of Polymer Miscibility

The effect of grafted-polymer miscibility (e.g., polymer hydrophobicity) on column selectivity and segment density profiles is shown in Fig. 8a,b, respectively. In a worse than theta solvent, such as when χ_{bo} = 1, the grafted polymer

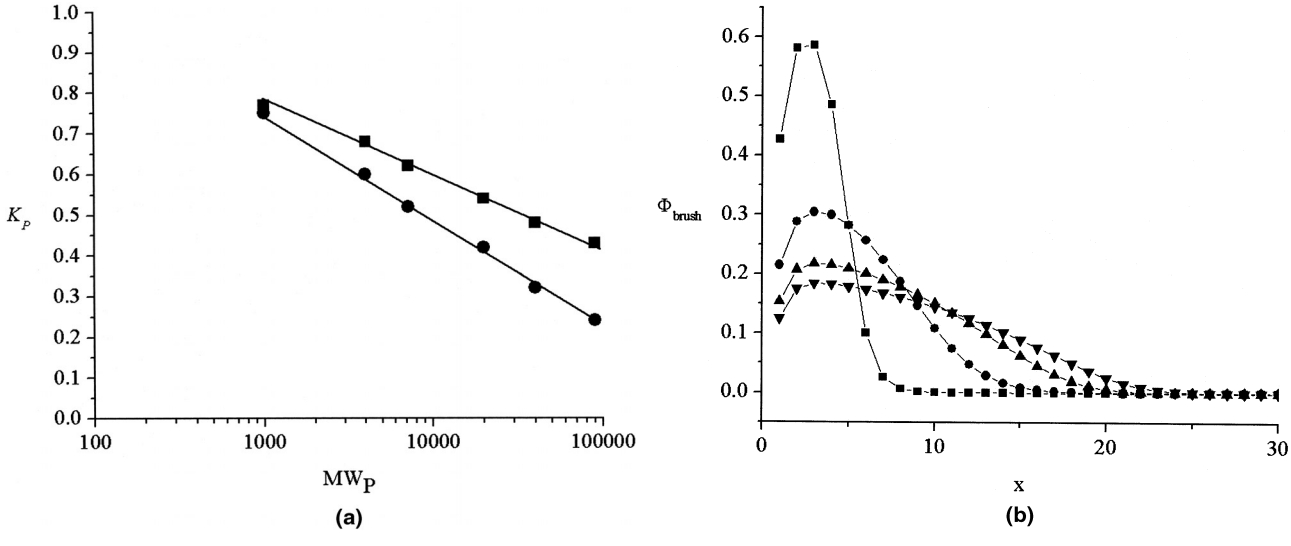

Figure 8. EIC column performance as a function of polymer brush miscibility in the mobile-phase solvent. **a:** SCF-EIC model predictions of the dependence of column selectivity on κ_{bo} (σ = 5%, N_{brush} = 50, κ_{po} = 0.4, κ_{bp} = 0): κ_{bo} = 0.5 (filled squares), 0 (filled circles). **b:** Influence of brush-solvent interaction κ_{bo} on predicted segment density profiles for an undisturbed grafted-polymer brush (σ = 5%, N_{brush} = 50, κ_{po} = 0.4, κ_{bp} = 0): κ_{bo} = 1 (filled squares), 0.5 (filled circles), 0 (filled triangles), –0.5 (filled inverted triangles).

collapses into a dense surface layer in a manner similar to classic phase separation of aqueous polymer solutions. When the polymer is miscible in the solvent, brush extension into the solvent is predicted as the brush–solvent interaction changes from unfavorable (χ_{bo} = 0.5) to athermal (χ_{bo} = 0), resulting in a significant increase in brush height, a decrease in maximum segment density, and a more gradual change in $\Phi_{brush}(x)$. However, further improvement of the solvent ($\chi_{bo} < 0$) results in only a small increase in brush height. In good solvents, the energy required to stretch a chain into a more linear configuration scales with brush height squared, while the associated increase in polymer-segment free volume scales with brush height. Thus, the stretching penalty prohibits severe chain extension even in the best of solvents.

A flexible polymer chain acts as a random walk under theta solvent (χ_{bo} = 0.5) conditions, where the configurational entropy of the chain is a maximum. In a good solvent (e.g., χ_{bo} = 0), the chain adopts the shape of a self-avoiding random-walk as the chain stretches from the grafting surface to improve contact with the solvent. The overall configurational entropy of the chain is reduced by this process, and the brush therefore becomes less accepting of large MW solutes, which necessarily reduce the density of favorable interactions between the solvent and chain segments. We might therefore expect the sensitivity and therefore the selectivity of an EIC column to improve when operated in an athermal solvent. This is indeed the case (Fig. 8a). Decreasing χ_{bo} from 0.5 to 0 increases the slope of the selectivity curve by a factor of 1.5, suggesting that the performance of EIC can be improved over that reported here by identifying polymer chemistries and/or solvent conditions where the solvent–polymer interaction is athermal or near athermal.

CONCLUSIONS

Entropic Interaction Chromatography efficiently separates mixtures of proteins and other macromolecules on the basis of size by contacting them with a stationary phase comprised of an inert solid support bearing a uniform brush of linear end-grafted homopolymer. Partitioning of solute into the brush volume reduces the configurational entropy of the solute and brush in proportion to the size of the analyte. Thus, as with traditional size exclusion chromatography, solute elution volumes are near V_o for high molecular weight analytes and increase with decreasing solute molecular weight. Reduced plate heights in wide-pore EIC columns are very small, allowing for efficient separation as a function of solute size without significant peak spreading. Coupling of a self-consistent field model of the solute particle – end-grafted polymer brush interaction with a classic equilibrium-dispersion type chromatography model allows accurate prediction of protein elution profiles on wide-pore EIC columns, as well as rapid analysis of the effects of resin properties and operating conditions on column separation efficiency. The resulting SCF-EIC model predicts that EIC performance is sensitive to σ and N_{brush}, and can also be modulated by changing polymer chemistry to alter its miscibility with the mobile-phase solvent. Columns of lower grafting density (σ = 5%) are shown and predicted to provide efficient separation of protein mixtures over three decades of protein molecular weight. In contrast, high-density wide-pore EIC columns offer a potentially attractive means of removing low molecular weight analytes and may therefore find value in desalting applications.

The authors thank Merck Biosciences for assistance in designing some of the experiments reported here and in preparing the two EIC resins used in these studies. CAH is a recipient of the Canada Research Chair in Interfacial Biotechnology.

References

Alexander S. 1977. Adsorption of chain molecules with a polar head: a scaling description. J Phys (Paris) 38:977–987.

Allen T. 1981. Particle size measurement. London: Chapman and Hall. p 432–436.

Athalye AM, Gibbs SJ, Lightfoot EN. 1992. Predictability of chromatographic protein separations — study of size-exclusion media with narrow particle size distributions. J Chromatogr 589:71–85.

Barackman J, Prado I, Karunatilake C, Furuya K. 2004. Evaluation of on-line high-performance size-exclusion chromatography, differential refractometry, and multi-angle laser light scattering analysis for the monitoring of the oligomeric state of human immunodeficiency virus vaccine protein antigen. J Chromatogr A 1043:57–64.

Barth HG, Jackson C, Bayer BE. 1994. Size exclusion chromatography. Anal Chem 66:595–620.

Bertolini J, Gomme P, Thomas P. 2004. Large-scale protein chromatography. Methods Mol Biol 251:211–224.

Bristow PA, Knox JH. 1977. Standardization of test conditions for HPLC columns. Chromatographia 10:279–289.

Brooks DE, Müller W. 1996. Size-exclusion phases and repulsive protein–polymer interaction/recognition. J Mol Recognit 9:697–700.

Brooks DE, Haynes CA, Hritcu D, Steels BM, Muller W. 2000. Size exclusion chromatography does not require pores. Proc Natl Acad Sci U S A 97:7064–7067.

Chakrabarti A, Toral R. 1990. Density profile of terminally anchored polymer chains: a Monte Carlo study. Macromolecules 23:2016–2021.

Cosgrove T, Heath T, Ryan G, van Lent B. 1987. The conformation of adsorbed poly(ethylene oxide) at the polystyrene/water interface. Polymer Commun 28:64–65.

Cosgrove T, Heath TG, Phipps JS, Richardson RM. 1991. Neutron reflectivity studies of polymers adsorbed on mica from solution. Macromolecules 24:94–98.

Curling JM. 1980. Methods of plasma protein fractionation. London: Academic Press.

Danckwerts PV. 1953. Continuous flow systems. Chem Eng Sci 2:1–9.

De Gennes PG. 1976. Scaling theory of polymer adsorption. J Phys (Paris) 37:1443–1452.

Dondi F, Cavazzini A, Remelli M, Felinger A, Martin M. 2002. Stochastic theory of size exclusion chromatography by the characteristic function approach. J Chromatogr A 943:185–207.

Dubin PL, Principi JM. 1989. Optimization of size-exclusion separation of proteins on a Superose column. J Chromatogr 479:159–164.

Field JB, Toprakcioglu C, Ball RC, Stanley HB, Dai L, Barford W, Penfold J, Smith G, Hamilton W. 1992. Determination of end-adsorbed polymer density profiles by neutron reflectometry. Macromolecules 25:434–439.

Friedli H, Kistler P. 1970. Polymers in preparation of human serum albumin. Vox Sang 18:542–546.

Goetz H, Kuschel M, Wulff T, Sauber C, Miller C, Fisher S, Woodward C. 2004. Comparison of selected analytical techniques for protein sizing, quantitation and molecular weight determination. J Biochem Biophys Methods 60:281–293.

Gooding KM, Regnier FE. 1990. HPLC of biological macromolecules. New York: Marcel-Dekker.

Guiochon G, Golshan-Shirazi S, Katti AM. 1994. Fundamentals of preparative and nonlinear chromatography. Boston: Academic Press.

Guo X, Condra M, Kimura K, Berth G, Dautzenberg H, Dubin PL. 2003. Determination of molecular weight of heparin by size exclusion chromatography with universal calibration. Anal Biochem 312:33–39.

Hagel L. 1989. Gel filtration. In: Janson JC, Ryden L, editors. Protein purification principles: high-resolution methods and applications. New York: John Wiley & Sons. p 63–105.

Horneman DA, Wolbers M, Zomerdijk M, Ottens M, Keurentjes JT, van der Wielen LA. 2004. Surfactant-aided size exclusion chromatography. J Chromatogr B 807:39–45.

Janson JC. 1971. Columns for large-scale gel filtration on porous gels: fractionation of rape seed proteins and insulin. J Agric Food Chem 19:581–588.

Janson JC, Jonsson J-Å. 1998. Introduction to chromatography. In: Janson JC, Ryden L, editors. Protein purification: principles, high-resolution methods, and applications, 2nd ed. New York: John Wiley & Sons.

Johnston A, Adcock W. 2000. The use of chromatography to manufacture purer and safer plasma products. Biotechnol Genet Eng Rev 17: 37–70.

Knox JH, Laird GE, Raven PA. 1976. Interaction of radial and axial dispersion in liquid chromatography in relation to the "infinite diameter" effect. J Chromatogr 122:129–137.

Ladisch MR. 2001. Bioseparations engineering. New York: Wiley-Interscience. p 308–313.

Lai PY, Binder K. 1992. Structure and dynamics of polymer brushes near the θ point: a Monte Carlo simulation. J Chem Phys 97:586–595.

Lin JJ, Meyer JD, Carpenter JF, Manning MC. 2000. Stability of human serum albumin during bioprocessing: denaturation and aggregation during processing of albumin paste. Pharm Res 17:391–396.

Lindquist U, Williams G. 1973. Isolation, purification, and determination of some chemical and physicochemical characteristics of alpha s-casein. J Dairy Sci 56:171–176.

Mathew E, Mirza A, Menhart N. 2004. Liquid-chromatography-coupled SAXS for accurate sizing of aggregating proteins. J Synchrotron Radiat 11:314–318.

Murat M, Grest GS. 1996. Molecular dynamics simulations of the force between a polymer brush and an AFM tip. Macromolecules 29: 8282–8284.

Ogston AG. 1958. The spaces in a uniform random suspension of fibres. Trans Faraday Soc 54:1754–1757.

Porath J, Flondin P. 1959. Gel filtration: a method for desalting and group separation. Nature 183:1657–1659.

Scheutjens JMHM, Fleer GJ. 1979. Statistical theory of the adsorption of interacting chain molecules. 1. Partition function, segment density distribution, and adsorption isotherms. J Phys Chem 83: 1619–1635.

Scheutjens JMHM, Fleer GJ. 1980. Statistical theory of the adsorption of interacting chain molecules. 2. Train, loop and tail size distribution. J Phys Chem 84:178–190.

Squire PG. 1964. A relationship between the molecular weights of macromolecules and their elution volumes based on a model for sephadex gel filtration. Arch Biochem Biophys 107:471–478.

Steels BM, Koska J, Haynes CA. 2000a. Analysis of brush-particle interactions using self-consistent-field theory. J Chromatogr B 743:41–56.

Steels BM, Leermakers FA, Haynes CA. 2000b. Analysis of compression of polymer mushrooms using self-consistent field theory. J Chromatogr B 743:31–40.

Tyn MY, Gusek TW. 1990. Prediction of diffusion coefficients of proteins. Biotechnol Bioeng 35:327–338.

Van Deemter JJ, Zuiderweg FJ, Klinkenberg A. 1956. Longitudinal diffusion and resistance to mass transfer as causes of non-ideality in chromatography. Chem Eng Sci 5:271–279.

Wu C. 1999. Column handbook for size exclusion chromatography. New York: Academic Press.

Yao Y, Lenhoff AM. 2004. Determination of pore size distributions of porous chromatographic adsorbents by inverse size-exclusion chromatography. J Chromatogr A 1037:273–282.

Yau W, Kirkland J, Bly D. 1979. Modern size exclusion chromatography. New York: Wiley Interscience.

Yau W, Kirkland J, Bly D. 1989. Size exclusion chromatography. In: Brown PR, Hartwick RA, editors. Chemical analysis: high performance liquid chromatography. New York: Wiley Interscience. p 293–295.